Int J Adv Manuf Technol (2016) 83:33–41
DOI 10.1007/s00170-015-7514-3

ORIGINAL ARTICLE

Feature selection for surface defect classification of extruded aluminum profiles

Apostolos Chondronasios[1] · Ivan Popov[1] · Ivan Jordanov[1]

Received: 22 October 2014 / Accepted: 30 June 2015 / Published online: 19 July 2015

Abstract This research investigates detection and classification of two types of the surface defects in extruded aluminium profiles; blisters and scratches. An experimental system is used to capture images and appropriate statistical features from a novel technique based on gradient-only co-occurrence matrices (GOCM) are proposed to detect and classify three distinct classes; non-defective, blisters and scratches. The developed methodology makes use of the Sobel edge detector to obtain the gradient magnitude of the image (GOCM). A comparison is made between the statistical features extracted from the original image (GLCM) and those extracted from the gradient magnitude (GOCM). This paper describes in detail every step of the image processing with example pictures illustrating the methodology. The features extracted from the image processing are classified by a two-layer feed-forward artificial neural network. The artificial neural network training is tested using different combinations of statistical features with different topologies. Features are compared individually and grouped. Results are discussed, achieving up to 98.6 % total testing accuracy.

Keywords Aluminum surface · Defect classification · Image gradient · Co-occurrence matrix · Neural network

✉ Apostolos Chondronasios
apostolos.chondronasios@port.ac.uk

Ivan Popov
ivan.popov@port.ac.uk

Ivan Jordanov
ivan.jordanov@port.ac.uk

[1] School of Engineering, University of Portsmouth, Portsmouth PO1 3DJ, UK

1 Introduction

The aluminum 6000 series of alloys have as primary alloying elements magnesium (Mg) and silicon (Si). They are used extensively for extrusions today because they have good corrosion resistance, surface finish, formability and medium strength, thus they can be perfect candidates for architectural sections and structural applications. Magnesium silicide (Mg_2Si) makes the 6000 alloys heat treatable and capable of achieving medium strength in the T6 condition [23].

The extrusion process is a complex one with many variables, some can be controlled (temperature, extrusion speed, lubrication) while others cannot. The final product is affected by those variables, resulting in different characteristics. Some of those characteristics appear on the surface in forms of defects (undesired results). The surface defects found in the literature are blisters, die-lines, pick-up, tearing, color streaks, weld lines, black lines and scratches [1, 19]. Some of those defects are exaggerated after anodizing or powder coating. The die and its quality are the most important factors of surface quality (and also geometry). This research paper will focus on blisters and scratches. Blistering is a result of entrapped air or lubricants below the surface. The contaminants can be trapped during upsetting due to the difference in diameter of the billet and the container. When temperature rises locally (due to friction), the gas expands and forms a blister [20, 23]. According to Sheppard, a *'burp cycle'* is often used to prevent this phenomenon by removing the ram pressure momentarily after upset to allow the air to escape [23]. Scratches are made during the handling of the extruded products by human error. They appear as a long line on the aluminum surface with a certain depth, which is the result of material being removed from the surface and are detrimental

to the quality when the extruded aluminum is painted (powder coated or anodized). The layer of paint is uneven and can lead to severe discolorations due to its varying thickness.

Machine vision is tailored to the particular inspection application, thus the possibilities of integration are endless. Over the past two decades, many machine vision systems have been installed in different areas for quality inspection. Image analysis techniques have already been applied for automated visual inspection, product quality control and materials characterization of a variety of products in industry. For the metalworking industry, extruded aluminum surfaces have not received a lot of attention. Extruded aluminum can be described as highly reflective, which leads to problems with illumination. A review about illumination techniques on metallic surfaces and application selection was conducted by Pernkopf and O'Leary, and suggests intensity imaging in this case [16]. A recent research on aluminum surface quality inspection was performed by Garbacz and Giesko [4]. In this research, without publishing any results, they discussed about possible ways of detecting defects with a strong emphasis on surface temperature distribution via an infrared camera. On a similar subject, Caleb-Solly and Smith have created an adaptive surface inspection system via interactive evolution [2]. The systems was applied in the hot-rolled steel industry and amongst the techniques used are image segmentation, self organizing map neural network, multi-layer perceptron classifier and evolutionary algorithms. Thresholding techniques are widely used in the literature to segment regions of interest. It is a technique that is widely used for automated visual inspection of defects. In real-world inspection cases, defects are either present of absent; they can also have a wide variety of sizes, creating a diversity not easily countered by thresholding techniques. One of the widely used automated thresholding technique is the Otsu method [15]. Ng was not satisfied with the results provided by this method for small defects, so he modified it developing the valley-emphasis method [12]. Especially for scratches in metal sheets, the valley-emphasis had 0.006 misclassification errors while Otsu had 0.192. Using similar methods, Shafeek et al. have written their own program in Microsoft Visual C++ for assessing defects in radio-graphs of welds [21]. Their method consisted of the following steps; histogram stretch, histogram equalization, median filter, histogram specification, thresholding, chain code algorithm, defect extraction. Performing a blob analysis, they were able to measure the area, perimeter, length and width of the defects with camera calibration (each pixel corresponded to 123 m). Zheng et al. approached the inspection of metallic surface defects in aluminum casting samples, with 91 % accuracy for hole defects and 86 % accuracy for crack defects; using genetic algorithms in combination with median filter, closing top-hat operation, segmentation threshold operation and noise removal via elimination of areas smaller than a defined value [29]. Jia et al. developed a defect detection system for the steel industry capable of detecting a defect in less than 6msec for one megabyte image [9]. They used a rough filtering algorithm based on a horizontal gradient operator to detect the edges of the seams on the hot rolled steel. Support vector machine algorithms were trained to learn complex decision boundaries in the presence of noise. Xue-Wu et al. developed a system for inspection of surface defects on strongly reflective metals [28]. They used wavelet transformations along with Sobel filter and thresholding to obtain five features from texture spectral measures of copper strips. The classification was done with a support vector machine and with an accuracy of 76.8 to 91.3 %.

Investigating techniques found in literature focused on heavily textured materials such as cork, glass surfaces, solar wafers and textiles; many important contributions are made during the last decade. Georgieva and Jordanov investigated a sample dataset of 700 cork tiles, which were used to produce a set of 33 features, using co-occurrence matrices measures and Law's filter masks [5]. Principal component analysis (PCA) and linear discriminant analysis (LDA) techniques were used and compared to reduce the dimensionality of the problem, along with $GLP\tau S$ training method for neural networks resulting in a testing success rate of up to 95 % for seven different sample classes. A further investigation by Petrov et al., using part of the same dataset and additional features such as Entropy, tested the performance of self-organizing maps with success rates up to 88 % on PCA and 98 % on LDA [18]. Concerning cork classification, Oliveira et al. used stepwise discriminant analysis to build predictive classification models to characterize the surface of cork stoppers and cluster them into three quality classes, analyzing the contribution of each porosity feature in the classification [13]. A difficult task was for Tsai and Chao to detect defects in sputtered glass surfaces, since the nature of those surfaces is random and anomalies are observed [25]. They developed an improved anisotropic diffusion scheme, specifically tailored for detecting defects, which smooths the background texture and preserves those anomalies of the in-homogeneously textured surfaces. The anisotropic diffusion scheme was first presented by Perona and Malik [17]. Tsai and Chao's method was superior to Gaussian and median filters because it did not falsely detect defects in clear surfaces and was also accurate at detecting them without including too many noisy pixels. The same technique, anisotropic diffusion, was used by Tsai et al. for the inspection of micro-cracks in heterogeneously textured solar wafers [26]. They modified the approach by subtracting the diffused image from the original gray-level image. The earlier approach was to smooth the original gray-level image and enhance the defective region in the diffused image. On the subject of fabrics,

Kumar has surveyed 166 sources for computer vision based defect detection and classification, providing an exhaustive review on the different methods used to approach classification [10]. Such methods for fabric defect detection were also reviewed by Shanbhag et al. [22]. Ortiz-Jaramillo et al. evaluated different texture classification methods, commonly used by researchers in the field, and provided results with good evidence that power spectrum, local binary patterns, the texture spectrum, Gaussian Markov random fields, auto-regressive models and the pseudo-Wigner distribution are good measures of fine changes in global texture [14].

For this investigation, a data set of 145 extruded aluminum surface images was collected. Three classes, non-defective, blister and scratches, are defined and attempts are made to classify them with high accuracy suitable for industrial application. Further investigation is made on feature selection and the resulting accuracy. Section 2 briefly covers the inspection system, illumination, image acquisition; discusses the methodology, while providing example figures, the equations used and a step by step procedure to follow the proposed approach to feature extraction. Section 2 covers the results from the combinations of different features and resulting ANN topologies. Finally, Section 4 concludes this paper and provides directions for improving this research.

2 Methodology

2.1 The typical inspection system

The typical components of a machine vision system include [3]:

- One or more digital cameras;
- Illumination suitable for the application;
- A processor which can be either a general purpose PC or a DSP;
- Sensors which trigger certain actions or trigger upon certain conditions
  (to start or stop acquiring images, to alarm the operator, to reject a defective part, etc);
- Machine vision software (either a commercially available package or a complete scratch build incorporating pattern recognition and classification methods);
- Data storage.

2.2 Aluminum defect inspection issues and considerations

The reflective properties of aluminum are to be considered, limiting the illumination options. A suitable system must enhance the defects and provide as little noise as possible to the captured image. Intensity imaging should be used as per Pernkopf's and O'Leary's suggestions [16].

Another consideration is the speed of the extrusion which is ranging from 5 to 80 m/min. Therefore, suitable cameras with adequately fast frame rate should be used when capturing images during the extrusion process (on-line). The cameras can be of either type: area scan or line scan, but to select the optimal performance type, additional considerations are necessary to choose the appropriate frame rate, process speed, captured area (for area scan), etc.

2.3 Image acquisition

The cameras, the lenses and the illumination system are the core of the image acquisition system. Each of the components has to be selected to match the requirements of the specific application and to complement each other. The purpose of the camera is to provide the resolution needed to detect defects and the frame rate to match the speed of the moving aluminum profile. For our application, a Basler Scout 1 mega-pixel gray-scale camera was used. The camera uses a CCD (charged-coupled device) sensor which is widely adopted in the industry because of its reliability and low cost.

For the purpose of this research, the samples were provided by a local company specialized in aluminum extrusions in a precut length of approximately 30 cm. The system consisted of fluorescent illumination, extending lengthwise more than the sample size, parallel to the direction of extrusion. The whole capturing system was enclosed in a box with the camera and the illumination to avoid environmental light pollution. A polarizer had to be fitted to the camera lens to suppress the polarized light. It was impossible to have an on-line capturing system due to the lack of necessary resources, so the whole process was done offline focusing strictly on the methodology.

2.4 Image capture

The procedure starts by reading the image from the camera or the disk drive. The picture is converted to gray-scale image using 8bit precision, which translates into 256 possible gray-scale value variations (0 to 255, with 0 being black and 255 white). The image is then separated in multiple regions of interest (RoI) of fixed width and length. This method allows for precise recognition as it identifies the position on the workpiece of the possible defects on the aluminum surface. For example, if an image is 1000 pixels wide, it can be separated into 10 RoIs having a width of 100 pixels. Similar segmentation is made for the length of the image. Thus, if a defect is identified the operator will be notified of its location on the workpiece.

Table 1 Low-pass filter 3x3

1	1	1
1	1	1
1	1	1

2.5 Noise removal and gradient magnitude calculation

On the next step, the gray-scale image is convoluted with a low-pass filter size 3 *x* 3. The convolution with a low-pass filter is used to remove noise from the image. Convolution is a process of multiplying two arrays of numbers of different sizes (most of the times) to produce a third array with the same dimensionality as the original. The first array is the gray-scale RoI. The second array is called the 'kernel'. In this algorithm, a 3 *x* 3 low-pass filter is used as shown in Table 1.

Following the noise removal, a Sobel edge detection operator is used (Fig 1). Two kernels are used in the Sobel operator (Table 2) [6, 24]. The edge magnitude obtained by the Sobel operator will be used to calculate the features of the sample data. The calculation is done using Eqs. 1 and 3, instead of using Eq. 2 which is the most used, Sobel suggests that the mathematically correct way is to divide **G** by 4, although a loss of low order significant bits can occur [24]. The image gradients were converted to uint8 format (converted to integers) in order to be useful in processing statistical features of co-occurrence matrices.

$$\mathbf{G}_x = \begin{bmatrix} -1 & 0 & +1 \\ -2 & 0 & +2 \\ -1 & 0 & +1 \end{bmatrix} * \mathbf{A} \quad \text{and} \quad \mathbf{G}_y = \begin{bmatrix} +1 & +2 & +1 \\ 0 & 0 & 0 \\ -1 & -2 & -1 \end{bmatrix} * \mathbf{A}, \tag{1}$$

where **A** is the original image.

$$\mathbf{G} = \sqrt{\mathbf{G}_x{}^2 + \mathbf{G}_y{}^2} \tag{2}$$

$$\mathbf{G} = \frac{|\mathbf{G}_x| + |\mathbf{G}_y|}{4} \tag{3}$$

2.6 Statistical GLCM features

The feature set for the sample classification is extracted from typical measures of co-occurrence matrices, but the proposed methodology requires it to be extracted from the gradient magnitude, which is a result of the Sobel operator. Co-occurrence matrices are a commonly applied statistical approach for texture feature extraction that considers relative distances and orientation of pixels with co-occurring values [3, 5, 7, 8]. A co-occurrence matrix is a matrix that is

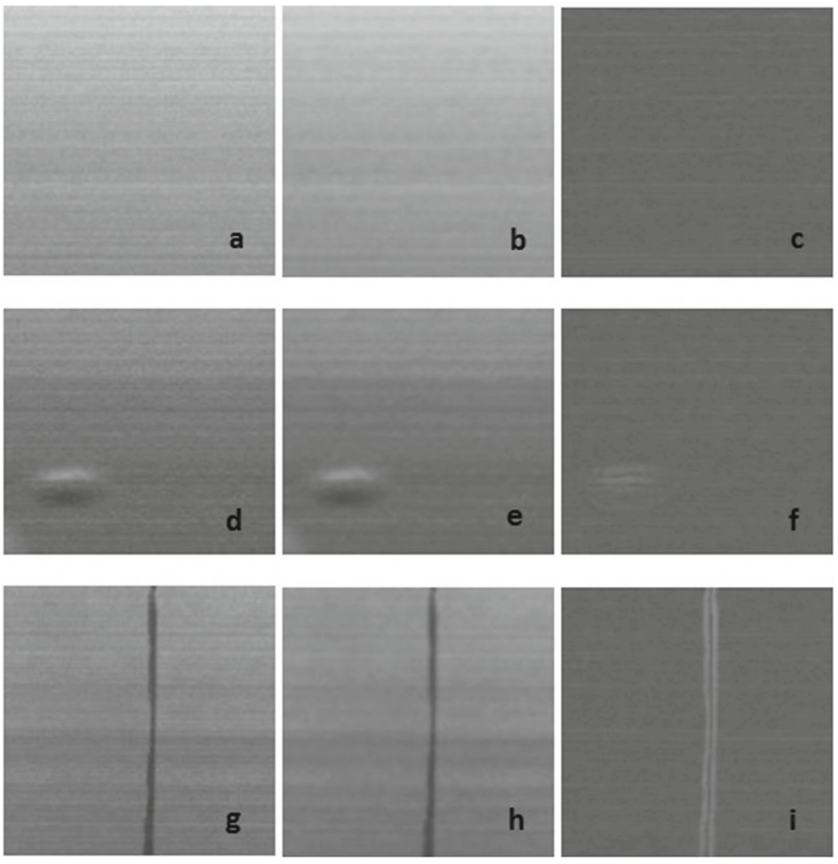

Fig. 1 Non-defective surface (**a**), blister defect (**d**), scratch defect (**g**) with their transformations after noise removal (**b**, **e**, **h**) and Sobel edge magnitude (**c**, **f**, **i**) (the Sobel images are brightness enhanced by 30 % for clarity)

Table 2 The kernels of the Sobel operator, for horizontal changes on the left and vertical on the right

-1	0	1
-2	0	2
-1	0	1

1	2	1
0	0	0
-1	-2	-1

defined over an image to be the distribution of co-occurring values at a given offset and direction. Mathematically, a co-occurrence matrix C is defined over an $n * m$ image I, parametrized by an offset $(\Delta x, \Delta y)$, as:

$$C_(\Delta x, \Delta y)(i, j) = \sum_{p,q=1}^{N,M} \begin{cases} 1 & \text{if } I(p,q) = i \quad \text{and} \\ & I(p + \Delta x, q + \Delta y) = j \\ 0 & \text{otherwise} \end{cases} \tag{4}$$

where i and j are the image intensity values, p and q are the spatial positions in the image I and the offset $(\Delta x, \Delta y)$ depends on the direction θ used and the distance d at which the matrix is computed. The value of the image is originally referred to the gray-scale value of the specified pixel, but it could be anything, from a binary 0/1 value to 32bit color and beyond.

Properties are such as *Contrast, Homogeneity, Energy and Correlation* are derived from co-occurrence matrices. This research uses combinations of those properties as features of the neural network input. An optimal combination will be selected in the following section. The first property, $Contrast$, measures the intensity contrast between neighboring pixels. $Homogeneity$ measures the closeness of the distribution of elements in the co-occurrence matrix to its diagonal. $Energy$ calculates the sum of squared elements in the co-occurrence matrix and $Correlation$ measures the linear dependency of grey levels on neighboring pixels. For the purposes of our research, those four features were used with directions of 0 and 90° and a spatial relationship of neighboring pixels ($d = 1$) in both directions, with the gray values scaled to a 6bit depth (2^6), resulting in $N = M = 64$ for the following equations.

$$\text{Contrast} = \sum_{i,j}^{N,M} (i - j)^2 C_{i,j} \tag{5}$$

$$\text{Homogeneity} = \sum_{i,j}^{N,M} \frac{C_{i,j}}{1 + (i - j)^2} \tag{6}$$

$$\text{Energy} = \sum_{i,j}^{N,M} C_{i,j}^2 \tag{7}$$

$$\text{Correlation} = \sum_{i,j}^{N,M} \frac{(i - \mu_i)(j - \mu_j)C_{i,j}}{\sigma_i \sigma_j} \tag{8}$$

2.7 Novel feature extraction process–GOCM

In summary, the process followed to extract features using the proposed methodology is:

- Remove noise. A Low-pass filter was used.
- Calculate the gradient magnitude. The Sobel method is a generally accepted good performing method. For the calculation of the gradient, Eq. 3 was used.
- Convert the gradient magnitude to integer values. Unsigned 8bit integer was used.
- Compute the co-occurrence matrix from the integer gradient magnitude.
- Extract the statistical features needed for the application. In this research, we calculated four of the proposed Haralick's features [8].

It is very crucial to convert the gradient to an integer because it is impossible to calculate a co-occurrence matrix when values are numbers with decimal points. The

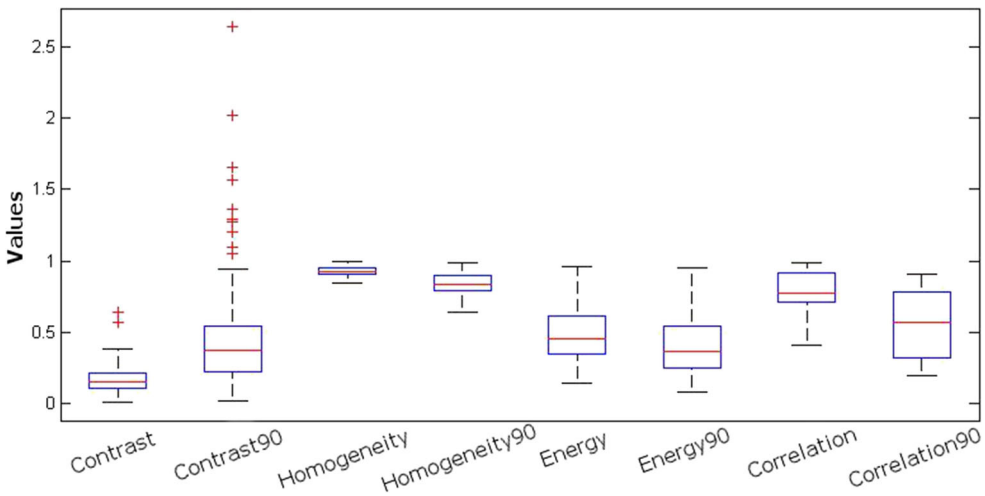

Fig. 2 Box-and-whisker diagram of the feature matrix

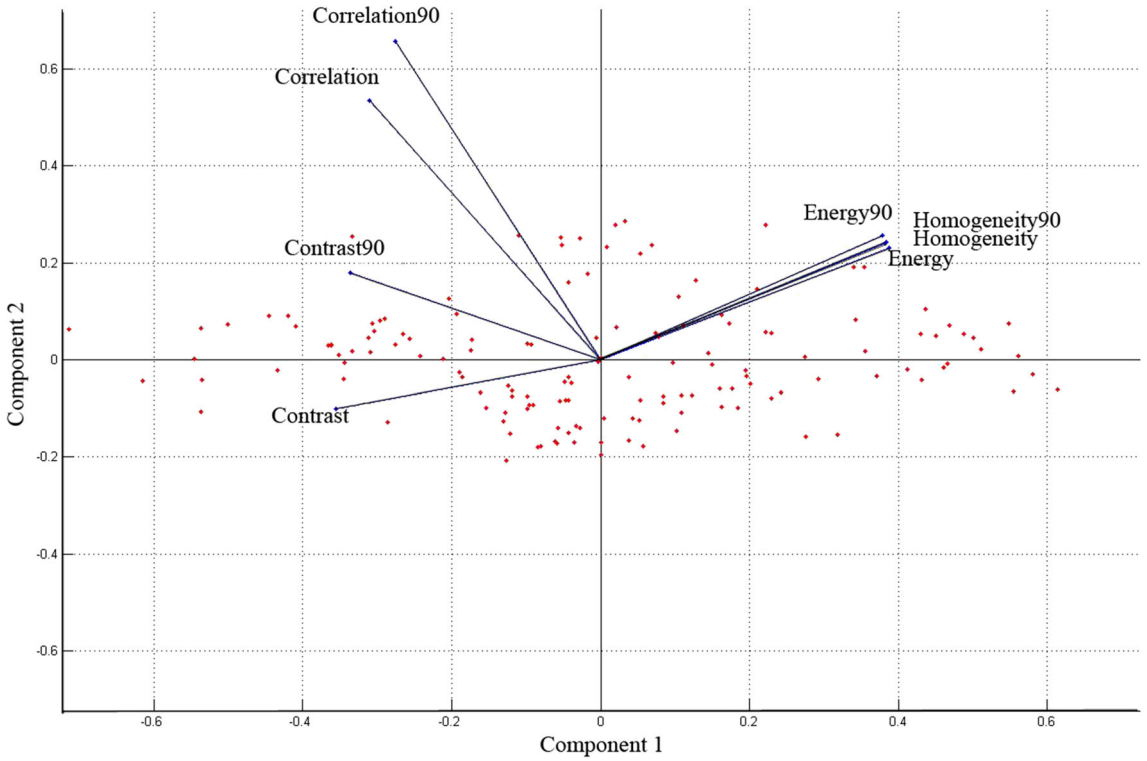

Fig. 3 Bi-plot of principal component coefficients and scores for first two principal components

proposed image conversion suggested by this research is uint8, unsigned 8bit integer, such as to correspond to the image's gray-level scale. To avoid confusion with existing spatial dependence matrices like gray level co-occurrence matrix (GLCM) and gray-level gradient co-occurrence matrix (GLGCM), we will call this matrix gradient-only co-occurrence matrix (GOCM). The difference between this and GLGCM is that the values i and j in our proposed method belong to the gradient of the image, while in GLGCM i belongs to the gray-level image and j belongs to the gradient [27].

2.8 Sample set

The sample set comprises of 145 images of 150 x 150 pixels in 8bit gray-scale with eight features each, distributed in three categories: non-defective (40 %), blisters (37 %) and scratches (23 %). The samples are surface images of industrial produced aluminum from a hot extrusion factory. MVTec Halcon version 9.0 (an industrial machine vision tool) was used to process the images and extract the feature matrix. Matlab version 2012b was used to process the feature matrix and allow different combinations of features to be used. The dataset was normalized to minimum and maximum values—1 and 1 respectively.

3 Experimental results

The box-and-whisker diagram represents the feature values (Fig 2); suggesting that $Homogeneity$ and $Homogeneity90$ are the least important features, which can be attributed to the low extend of the whiskers (their variance is the lowest). If the dimensionality of the problem was to be reduced, those are the first feature candidates to

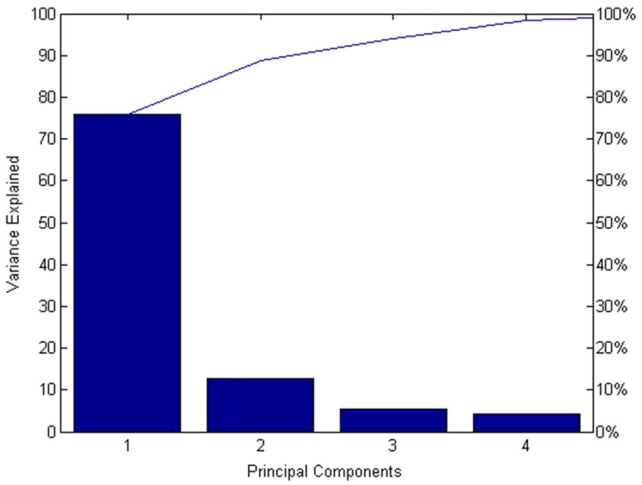

Fig. 4 Scree plot of the principal components with 95 % total variance

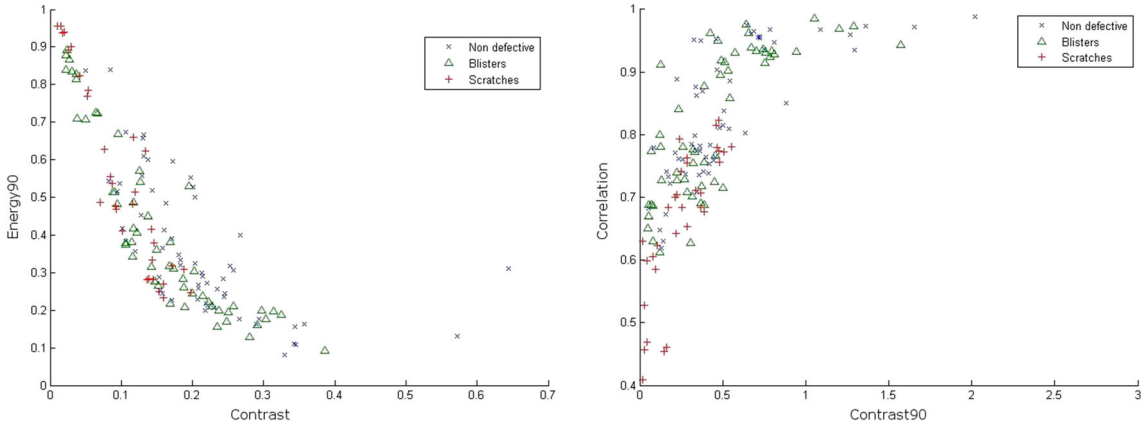

Fig. 5 Scatter plots of a random selection of features

consider eliminating. This can be further investigated using principal components analysis and exploring how the features affect the most important principal components. The scree plot (Fig. 4) depicts the principal components that explain 95 % of the total variance.

The first principal component accounts for 75.99 % of the total variance and the second component for 12.72 %, to a sum total of 88.71 % of the total variance. From the bi-plot (Fig. 3), an observation can be made that *Energy*, *Energy90*, $Homogeneity$, $Homogeneity90$ have approximately the same effect on the first two principal components, due to same direction, approximately same vector size and similar angles.

The assumption from the previous evidence suggests that five features will give enough performance for the classification. Supposedly, the selection of $Contrast$, $Contrast90$, $Energy$, $Correlation$, $Correlation90$ will provide the same results as the full feature set of eight features. Prior to the classification, an investigation of whether the features are linearly separable or not has to be performed, in order to select an appropriate classification technique. One of the ways to present the results is via scatter plots, in which random features from all three classes were selected to be plotted against each other (Fig. 5). The data are non linearly separable suggesting that multi-layer perceptrons or support vector machines are possible candidates for successful classification.

The selected classification technique was two-layer feed forward neural network with sigmoidal transfer functions, utilizing a scaled conjugate algorithm [11]. The input was a 145x(1–8) matrix, 145 samples and (1–8) for the features, which was divided in two stages. The first stage was to keep 50 % of the data separate in order to retest each network's performance in presence of new data, while the second stage was to use the remaining data divided by 85 % for training and 15 % for validation. The same test sample group was kept separate from any training or validation for all the neural networks trained and tested in this research paper. This was done in order to have objective comparisons between the different neural network topologies and inputs. The topology used for testing each individual feature was 1-2-3 (first number is the input features, second is the hidden neurons, third is the outputs). The hidden layer size was tested empirically and $Inputs + 1$ was performing well in the experiments. The outputs were in binary format (1-0-0 for Non-Defective, 0-1-0 for Blisters and 0-0-1

Table 3 Artificial neural network topology table with MSE and accuracy values over an average of 100 tested ANNs for each feature

ANN topology	Features	GLCM		GOCM	
		MSE	Accuracy	MSE	Accuracy
1-2-3	$Contrast$	0.1900	56.2	0.1851	60.3
1-2-3	$Contrast90$	0.1790	61.6	0.1745	65.8
1-2-3	$Correlation$	0.1881	64.4	0.1186	78.1
1-2-3	$Correlation90$	0.1777	61.6	0.0859	87.7
1-2-3	$Energy$	0.2046	49.3	0.1781	63.0
1-2-3	$Energy90$	0.2023	53.4	0.1884	57.5
1-2-3	$Homogeneity$	0.1992	47.9	0.1861	61.6
1-2-3	$Homogeneity90$	0.2026	54.8	0.1935	56.2

Table 4 Artificial neural network topology table with MSE and accuracy values over an average of 100 tested ANNs for each feature group

ANN topology	Features	GLCM		GOCM	
		MSE	Accuracy	MSE	Accuracy
2-3-3	Cr,Cr90	0.1682	65.8	0.0353	98.6
3-4-3	Cr,Cr90,C	0.1631	63.0	0.0356	97.3
3-4-3	Cr,Cr90,C90	0.1568	63.0	0.0385	98.6
3-4-3	Cr,Cr90,E	0.1604	65.8	0.0456	97.3
3-4-3	Cr,Cr90,E90	0.1545	63.0	0.0385	97.3
3-4-3	Cr,Cr90,H	0.1656	64.4	0.0362	97.3
3-4-3	Cr,Cr90,H90	0.1697	63.0	0.0360	97.3
4-5-3	C,C90,E,E90	0.1579	64.4	0.1406	74.0
4-5-3	C,C90,H,H90	0.1452	71.2	0.1366	76.7
4-5-3	C,C90,Cr,Cr90	0.1490	65.8	0.0232	97.3
5-6-3	C,C90,E,Cr,Cr90	0.1218	78.1	0.0224	97.3
6-7-3	C,C90,H,H90,E,E90	0.1430	75.3	0.1229	82.2
6-7-3	C,C90,E,E90,Cr,Cr90	0.1287	78.1	0.0201	97.3
8-9-3	C,C90,H,H90,E,E90,Cr,Cr90	0.1182	79.5	0.0244	97.3

C contrast, $C90$ contrast90, E energy, $E90$ energy90, H homogeneity, $H90$ homogeneity90, Cr correlation, $Cr90$ correlation90

for Scratches). Before proceeding with the final results, the features were calculated individually using the traditional GLCM approach, where the features are extracted directly from the original image's statistical texture measures. To make a direct comparison, a calculation of the features from the edge magnitude of the image followed (GOCM). The results provided are over an average of 100 training sessions, with the average Mean Squared Error and Accuracy presented in Table 3.

The most interesting feature is $Correlation$ obtained using $\theta = 0°$, $d = 1$ and $\theta = 90°$, $d = 1$. The $Correlation$, $Correlation90$ and $Contrast90$ obtained from GLCM provide the highest accuracy, which implies they are the strongest features. Similar performance to those features is obtained from $Contrast$, $Contrast90$, $Energy$ and $Homogeneity$ in the GOCM case. $Correlation$ and $Correlation90$ have exceptionally high accuracy when they derive from the edge magnitude.

Table 4 summarizes the tested networks with the statistical features' combinations and resulting topologies. The best performing combination of GLCM features is 8-9-3 with an accuracy of 79.5 %. It is observed that the accuracy increases while more features from the GLCM are introduced. On the contrary, there is an interesting observation to be made for GOCM features, $Correlation$ and $Correlation90$ in pair are the best performing combination regarding accuracy 98.6 %. None of the other combinations achieves this high accuracy because the information provided by the other data proves to be redundant. The computational load for each image of 150x150 pixels using 6bit scale for the eight statistical features of GOCM matrices with the Sobel calculation for the gradient was on average 30 ms on an Intel 4770 k processor at 4.1 GHz.

4 Conclusions—discussion

In this paper, a computer vision-based system for inspection of surface defects on aluminum profiles was developed. The study focused on two defects, blisters and scratches, and classified them in three classes (non-defective, blister, scratch). We performed a feature selection for this application, which resulted in 98.6 % accuracy using only two features. This high detection accuracy is achieved combining the current literature on the field with a novel approach on selecting and manipulating variables, such as obtaining values from the statistical features of co-occurrence matrices on the gradient magnitude of the image as a result of the Sobel operator. We called this matrix GOCM to be able to distinguish it between the traditional GLCM and GLGCM approaches. Even if the nature of the aluminum surface texture is near-stochastic, which makes defect detection especially difficult, we have proven that using statistical features from the GOCM is more suitable in extruded aluminum surface inspection.

This research can be further enriched by adding more samples for different types of defects such as die-lines, pick-up, tearing, color streaks, weld lines and black lines. For the classification of more defects, the accuracy is expected to drop when using only two features, because they will lose some of their discrimination ability. Different types of cameras and measuring equipment can be

used to obtain data able to distinguish better amongst similar type of defects. Another possibility of future research is to test the performance of different classification systems such as support vector machines and compare them to neural networks' performance. Last direction of future research, but not least important, would be to test the proposed GOCM methodology using standard texture benchmarks.

Acknowledgements This research was partially funded by EXALCO S.A., an aluminum extrusion company based in Greece, which kindly provided samples, hardware and software.

References

1. Arif A, Sheikh A, Qamar S, Raza M, Al-Fuhaid K (2002) Product defects in aluminum extrusion and their impact on operational cost. In: Proceedings of the 6th Saudi Engineering Conference, pp 137–154
2. Caleb-Solly P, Smith JE (2007) Adaptive surface inspection via interactive evolution. Image Vis Comput 25(7):1058–1072
3. Davies ER (2012) Computer and machine vision: theory, algorithms, practicalities, Academic Press
4. Garbacz P, Giesko T (2013) Inspection of aluminium extrusion using infrared thermography
5. Georgieva A, Jordanov I (2009) Intelligent visual recognition and classification of cork tiles with neural networks. IEEE Trans Neural Netw 20(4):675–685
6. Gonzalez RC, Woods RE (2002) Digital image processing. Prentice Hall, Upper Saddle River, NJ
7. Haralick RM (1979) Statistical and structural approaches to texture. Proceedings of the IEEE 67(5):786–804
8. Haralick RM, Shanmugam K, Dinstein IH (1973) IEEE Trans Syst Man Cybern 6:610–621
9. Jia H, Murphey YL, Shi J, Chang TS (2004) An intelligent real-time vision system for surface defect detection. In: Pattern Recognition, 2004. ICPR 2004. Proceedings of the 17th International Conference on, IEEE, vol 3, pp 239–242
10. Kumar A (2008) Computer-vision-based fabric defect detection: a survey. IEEE Trans Ind Electron 55(1):348–363
11. Møller MF (1993) A scaled conjugate gradient algorithm for fast supervised learning. Neural Netw 6(4):525–533. doi:10.1016/S0893-6080(05)80056-5
12. Ng HF (2006) Automatic thresholding for defect detection. Pattern Recogn Lett 27(14):1644–1649
13. Oliveira V, Knapic S, Pereira H (2013) Classification modeling based on surface porosity for the grading of natural cork stoppers for quality wines, Food and Bioproducts Processing
14. Ortiz-Jaramillo B, Orjuela-Vargas SA, Van-Langenhove L, Castellanos-Domnguez CG, Philips W (2014) Reviewing, selecting and evaluating features in distinguishing fine changes of global texture. Pattern Anal Applic 17(1):1–15
15. Otsu N (1975) A threshold selection method from gray-level histograms. Automatica 11(285–296):23–27
16. Pernkopf F, O'Leary P (2003) Image acquisition techniques for automatic visual inspection of metallic surfaces. NDT & E International 36(8):609–617
17. Perona P, Malik J (1990) Scale-space and edge detection using anisotropic diffusion. IEEE Trans Pattern Anal Mach Intell 12(7):629–639
18. Petrov N, Georgieva A, Jordanov I (2013) Self-organizing maps for texture classification. Neural Comput & Applic 22(7–8):1499–1508
19. Qamar S, Arif A, Sheikh A (2004) Analysis of product defects in a typical aluminum extrusion facility. Mater Manuf Process 19(3):391–405
20. Saha PK (2000) Aluminum extrusion technology. ASM International
21. Shafeek H, Gadelmawla E, Abdel-Shafy A, Elewa I (2004) Assessment of welding defects for gas pipeline radiographs using computer vision. NDT & E International 37(4):291–299
22. Shanbhag PM, Deshmukh M, Suralkar S (2012) Overview: methods of automatic fabric defect detection. Global Journal of Engineering, Design & Technology 1(2):42–46
23. Sheppard T (1999) Extrusion of aluminium alloys. Springer
24. Sobel I (1990) An isotropic 3 3 image gradient operator. Machine Vision for three-demensional Sciences
25. Tsai DM, Chao SM (2005) An anisotropic diffusion-based defect detection for sputtered surfaces with inhomogeneous textures. Image Vis Comput 23(3):325–338
26. Tsai DM, Chang CC, Chao SM (2010) Micro-crack inspection in heterogeneously textured solar wafers using anisotropic diffusion. Image Vis Comput 28(3):491–501
27. Wang-Cheung Lam S (1996) Texture feature extraction using gray level gradient based co-occurence matrices. In: Systems, Man, and Cybernetics, 1996., IEEE International Conference on, IEEE, vol 1, pp 267–271
28. Xue-Wu Z, Yan-Qiong D, Yan-Yun L, Ai-Ye S, Rui-Yu L (2011) A vision inspection system for the surface defects of strongly reflected metal based on multi-class svm. Expert Systems with Applications 38(5):5930–5939
29. Zheng H, Kong LX, Nahavandi S (2002) Automatic inspection of metallic surface defects using genetic algorithms. J Mater Process Technol 125:427–433